Data in Brief 41 (2022) 107845

Contents lists available at ScienceDirect

Data in Brief

journal homepage: www.elsevier.com/locate/dib

Data Article

3-D data of thermal regime, water content, and slab dehydration in Alaska

Rui Qu[a,b], Yingfeng Ji[a,b,*], Weiling Zhu[a,b,c]

[a] State Key Laboratory of Tibetan Plateau Earth System and Resources Environment (TPESRE), Institute of Tibetan Plateau Research, Chinese Academy of Sciences, Beijing 100101, China
[b] University of Chinese Academy of Sciences, Beijing 100049, China
[c] Department of Geophysics, Yunnan University, Kunming 650091, China

ARTICLE INFO

Article history:
Received 16 December 2021
Revised 10 January 2022
Accepted 13 January 2022
Available online 19 January 2022

Keywords:
Numerical simulation
Thermal regime
Water content
Slab dehydration

ABSTRACT

The data include the 3-D temperature field (degrees Celsius), water content (wt%), dehydration rate (wt%/km), and subduction velocity field (cm/yr) of the subducting plate, as well as the coastline and volcano distribution in Alaska. The data of the model region have dimensions of 800 × 1600 × 400 km (length × width × depth). The geometry of the subducted plate is well constrained by Slab2.0, and the plate ages are provided by EarthByte. The subduction velocities inside a prescribed 3-D constrained volume of the oceanic lithosphere are given based on the kinematic plate subduction modeling method and the MORVEL plate motion data. The observation of surface heat flow and Curie point depths are used to constrain the model thermal regime. The geophysical calculation is ensured after the subduction thermal regime reaches a steady state. Data are deposited in the TPDC repository, which has granted a persistent identifier https://data.tpdc.ac.cn/en/disallow/8b266d22-fea7-4259-9a5f-8ac0bd9e7869/. Data include (1) paraview_eq_USGS.vtk (earthquake catalog by IRIS, 2000-2010, Trabant et al., 2012), (2) paraview_slab.vtk (3-D thermal regime, slab water content and slab dehydration), (3) paraview_volcano.vtk (global volcanoes at NCEI, Siebert et al., 2010), and (4) paraview_map.vtk (coastline, GMT).

* Corresponding author.
E-mail address: yingfengji@itpcas.ac.cn (Y. Ji).

https://doi.org/10.1016/j.dib.2022.107845
2352-3409/© 2022 The Author(s). Published by Elsevier Inc. This is an open access article under the CC BY-NC-ND license (http://creativecommons.org/licenses/by-nc-nd/4.0/)

© 2022 The Author(s). Published by Elsevier Inc.
This is an open access article under the CC BY-NC-ND
license (http://creativecommons.org/licenses/by-nc-nd/4.0/)

Specifications Table

Subject	Geophysics
Specific subject area	Geodynamic numerical modeling
Type of data	Paraview vtk files data
How the data were acquired	The data was acquired through 3-D numerical thermal modeling which was developed from originally code stag3d. An anelastic liquid approximation and the equations of conservation of mass, momentum, and energy are used in this model. Based on a three-dimensional thermomechanical model (Ji et al. [1,2]) and the collect earthquake catalog from IRIS [3], the data of the slab thermal state, water content, and slab dehydration distribution in Alaska are calculated.
Data format	Paraview data format: vtk files The data includes the x, y, z coordinates, temperature (°C), water content (wt%), dehydration rate (wt%/km), and subduction velocity field (cm/yr) of the Nazca plate, as well as the coastline and volcano distribution in Alaska.
Description of data collection	The data coordinates are temporarily an orthogonal coordinate system, where the origin of the coordinates is (155.0 °W, 54.9 °N), the x+ azimuth is 150 degrees clockwise from the north, the y+ azimuth is 60 degrees clockwise from the north, and the z+ direction is vertical downward, in kilometers. The data source method is a three-dimensional finite-difference numerical simulation. The geophysical calculation is ensured after the subduction thermal regime reaches a steady state. The temperature field error range is ±10 degrees Celsius, and the velocity field error range is ±0.1 cm/yr. This data can be used to further analyze the geophysical field of the subduction zone.
Data source location	Country: USA-Alaska Latitude and longitude for collected data:172 °W-140 °W, 49 °N-65 °N
Data accessibility	TPDC repository (https://data.tpdc.ac.cn/en/disallow/8b266d22-fea7-4259-9a5f-8ac0bd9e7869/)
Related research article	Qu, R., Ji, Y., Zhu, W. (2021). Variations in wedge earthquake distribution along the strike underlain by thermally controlled hydrated megathrusts. Applied Sciences, 11, 7268. https://doi.org/10.3390/app11167268.

Value of the Data

- The data provide meaningful referential thermal regime, water content, and slab dehydration rate in Alaska for those who are interested.
- The data can be used to analyze the regional geophysical field of the subduction zone.
- Researchers from various disciplines of geoscience may take advantage of these data in 3-D model tests and 3-D exhibitions.
- Investigation of the 3-D hydrothermal regime could be helpful to understand the relationships between the seismic risks and subduction tectonics in Alaska.

1. Data Description

The data in Paraview format (vtk files) include the attributes of x, y, z coordinates, temperature (°C), water content (wt%), dehydration rate (wt%/km), and subduction velocity field (cm/yr) of the subducted plate and the distribution of the coastline and volcano in the model region. The coordinate data are in an orthogonal coordinate system, where the origin of the coordinates is (155.0 °W, 54.9 °N), the x+ azimuth is 150 degrees clockwise from the north, the y+ azimuth is 60 degrees clockwise from the north, and the z+ direction is vertical downward, in

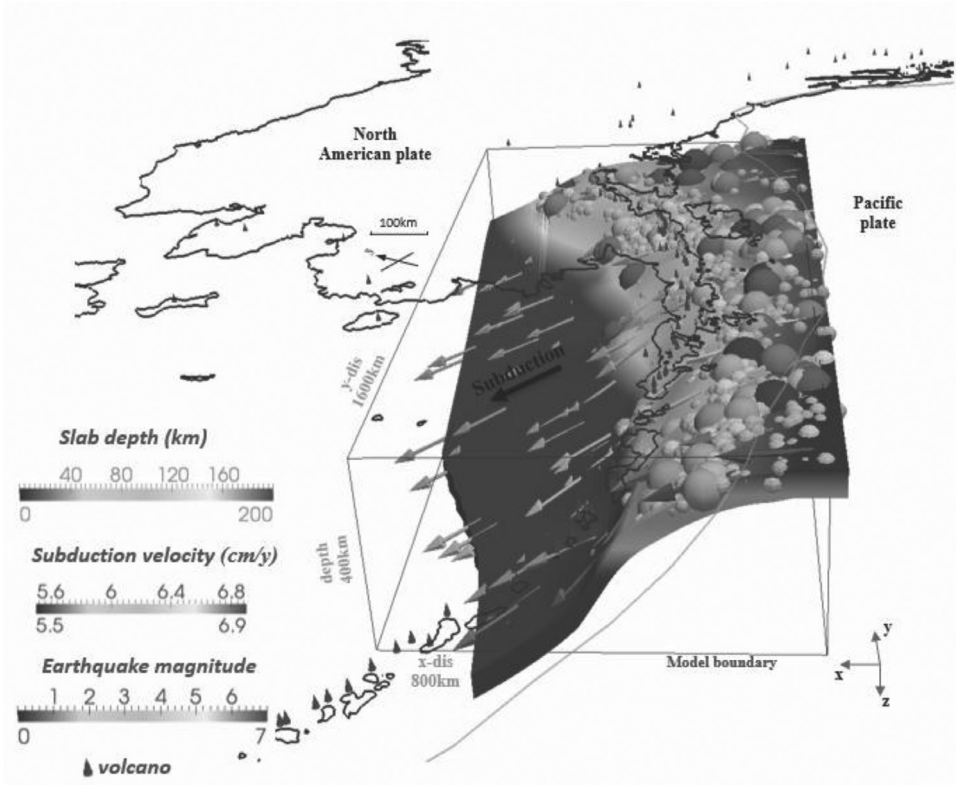

Fig. 1. The model settings and boundary conditions for the model. The seismic events are plotted in spheres. Cones indicate active arc volcanoes [11].

kilometers. The error range of the temperature field and velocity field is ca. ±10 degrees Celsius and ±0.1 cm/yr, respectively.

The data source method is a three-dimensional finite-difference numerical modeling method. Through 3-D numerical simulation of the thermal regime and water content of the Alaskan subduction zone, it becomes feasible to incorporate the 3-D geometric data of the incoming plate, which are updated through seismic tomography (Slab2) [4], and the real subduction velocities from the MORVEL [5] and NNR-MORVEL56 [6] datasets. The age data of the subducted plate are obtained following the oceanic seafloor age, which is estimated by the trenchward model boundary based on EarthByte [7]. The model dimensions are 1600 km × 800 km × 400 km (along-arc length × across-arc length × depth) and 80 × 80 × 100 grids (Fig. 1). The incoming oceanic plate is composed of a MORB layer at the top with a thickness of 17 km underlain by an ultramafic rock layer [8]. The oceanic lithosphere thickness is estimated according to Yoshii [9]. The temperature boundary condition agrees with the plate cooling model [10]. The bottom of the slab and the perpendicular plane are prescribed as adiabatic and permeable, and the top surface is set to be a fixed temperature (0 °C) and rigid (Fig. 1).

The subduction velocities inside a prescribed 3-D constrained volume of the oceanic lithosphere are given based on the kinematic plate subduction modeling method [1,2]:

$$v_x(x,y,z) = \frac{-2a(x,y)b(x,y)v_y + \sqrt{\{2a(x,y)b(x,y)v_y\}^2 - 4\{a(x,y)^2+1\}\left[\{a(x,y)^2+1\}v_y{}^2 - v^2\right]}}{2\{a(x,y)^2+1\}}, \quad (1)$$

$$v_y(x,y,z) = v_y, \quad (2)$$

$$v_z(x,y,z) = a(x,y)v_x + b(x,y)v_y, \quad (3)$$

while

$$a(x,y) = \frac{1}{2}\{Z(x+\Delta x,y) - Z(x-\Delta x,y)\} \cdot \frac{z_{max}}{x_{max}}, \quad (4)$$

$$b(x,y) = \frac{1}{2}\{Z(x+\Delta x,y+\Delta y) - Z(x+\Delta x,y) + Z(x-\Delta x,y) - Z(x-\Delta x,y-\Delta y)\} \cdot \frac{z_{max}}{y_{max}}. \quad (5)$$

Here, v is the subduction velocity, and Δ is the interval between two neighboring nodes along the axes. x_{max}, y_{max}, and z_{max} indicate the model lengths along the x-, y-, and z-axes, respectively.

According to Omori et al. [12] (MORB) and Hacker et al. [8], a P–T-wt%-facies database is established with a P–T grid interval of 0.04 GPa (1.2 km) and 5 °C. The temperature and pressure data at every P–T grid point are calculated from our 3-D thermomechanical model. The pressure (GPa) at every grid point is obtained by converting its depths (km) through PREM (preliminary reference earth model) parameters. Using the temperature and pressure provided by the numerical simulation, both each facies domain and the corresponding water content (wt%) at every grid are estimated. Through the interpolation method, the intraslab water content distribution (wt%) at various depths is then obtained.

Using the change in rock saturation water content (wt%) via a distance (km) in the subduction direction between neighboring grids, the inner-slab slab dehydration (wt%/km) is calculated. The slab is prescribed to be divided into >70 layers according to the mesh number, with the layer surface parallel to the plate interface. Then, the water content at a point on a layer surface was calculated from the water content at the grids surrounding this point through an interpolation method. Thus, the water content at each point on every layer surface is obtained. Next, the water content value difference between two neighboring points in the subduction direction is divided by the point distance (which can be derived using the horizontal distance and vertical distance), and then slab dehydration at each point on a layer can be obtained. Based on these steps, the intraslab dehydration distribution is well calculated. Slab minerals vary in saturation at each subduction stage. Thus, slab dehydration (wt%/km) reflects the efficiency of fluid production by crystalline breakdown and fluid relaxation during subduction.

2. Experimental Design, Materials and Methods

Aiming to investigate the in situ along-strike slab thermal variation on megathrusts and the geographically distributed hydrothermal state, a 3-D thermomechanical model was constructed based on code Stag3D [13] and the finite difference method. In this model, an anelastic liquid approximation and the equations of conservation of mass, momentum, and energy [1,2] are used:

$$\nabla \cdot \{\rho_s(z,T_s)\boldsymbol{v}\} = 0, \quad (6)$$

$$-\frac{\partial P}{\partial x_i} + \frac{\partial \tau_{ij}}{\partial x_j} - \delta_{i3}\rho_s g\alpha_0(T - T_s) = 0, \quad (7)$$

Table 1
Main model parameters.

	Model Parameters	Value	Units
ρ_0	Standard density	3300	kg•m^{-3}
α_0	Standard thermal expansion	3×10^{-5}	K^{-1}
T_0	Standard temperature	1600	K
k_0	Standard thermal conductivity	2.9	W•m^{-1}•K^{-1}
Hr	Radioactive heat generation rate in the mantle	2.245×10^{-13}	W•m^{-3}
C_{p0}	Standard specific heat at constant pressure	1200	J•kg^{-1}•K^{-1}
κ_0	Standard thermal diffusivity	7.6×10^{-7} [2]	m^2•s^{-1}
η_0	Standard viscosity	1×10^{20}	Pa•s
v	Subduction velocity	6.6-7.2 [5]	cm•yr^{-1}
		Diffusion Creep [14]	Dislocation creep [14]
n_0	Stress exponent	1.0	3.5
A_0	Pre-exponential factor	1.0	9.0×10^{-20}
C_{OH}	OH concentration (H/10^{6}Si)	1000	1000
r C_{OH}	exponent	1.0	1.2
E_0	Activation energy (kJ/mol)	335	480
V_0	Activation volume (m^3/mol)		
	Upper mantle	4.0×10^{-6}	11.0×10^{-6}
	Lower mantle	1.5×10^{-6}	-
d	Grain size (μm)		
	Upper mantle	10,000	-
	Lower mantle	40,000	-

$$\rho c_p\left(\frac{\partial T}{\partial t} + \boldsymbol{v}\cdot\nabla T\right) = k\nabla^2 T + \eta(\nabla v)^2 + \rho g\alpha T v_z + \rho H_r, \tag{8}$$

where P is the pressure deviation from hydrostatic pressure, α_0 is the reference thermal expansivity, τ_{ij} $(i,j = 1, 2, 3)$ is the stress tensor, and δ_{ij} is the Kronecker delta. The energy equation includes the advection term, thermal diffusion term, viscous dissipation term, adiabatic heating term, and radioactive heating term. The main model parameters are tabulated in Table 1.

The viscous flow law for wet olivine [14] following laboratory experiments is included in the model. The deformation of olivine occurs by both diffusion creep (df) and dislocation creep (ds), where each mechanism accommodates a portion of the total strain rate [15]:

$$\dot{\varepsilon}_t = \dot{\varepsilon}_{df} + \dot{\varepsilon}_{ds}. \tag{9}$$

The composite upper mantle viscosity for deformation at constant stress is

$$\eta_{comp} = \frac{\eta_{df}\eta_{ds}}{\eta_{df} + \eta_{ds}}. \tag{10}$$

Here, η_{df} and η_{ds} represent the diffusion creep and dislocation creep viscosities for olivine. The viscosity law is

$$\eta_{df,ds} = \left(\frac{d^p}{A_0 C_{OH}^r}\right)^{\frac{1}{n}} \dot{\varepsilon}_E^{\frac{1-n}{n}} \exp\left(\frac{E_0 + P_l V_0}{n_0 R T_a}\right), \tag{11}$$

where $\dot{\boldsymbol{\varepsilon}}_{\boldsymbol{E}} = (\frac{1}{2}\dot{\varepsilon}_{ij}\dot{\varepsilon}_{ij})^{\frac{1}{2}}$ is given by the square root of the second invariant of the strain rate tensor reported by Ranalli [16], A_0 is the preexponential factor, d is the grain size, p is the grain size exponent, C_{OH} is the OH concentration (H/10^{6}Si), r is the C_{OH} exponent, n and n_0 are the stress exponents, E_0 is the activation energy, V_0 is the activation volume, T_a is the temperature, including the adiabatic temperature gradient (3×10^{-4} K/m), R is the gas constant, and P_l is the lithostatic pressure [17]. The trenchward thermal structure follows the global depth and heat

(GDH1) model [10]:

$$T(z, t_{oc}) = T_m \left[\frac{z}{d_0} + \frac{2}{\pi} \sum_{n-1}^{\infty} \frac{1}{n} \sin\left(\frac{n\pi z}{d_0}\right) \exp\left(\frac{-n^2 \pi^2 \kappa t_{oc}}{{d_0}^2}\right) \right] \tag{12}$$

The time-dependent thermal boundary condition includes the initialization time. $T(z, t_{oc})$ is the temperature at depth z and plate age t_{oc} along the trench, T_m is the lithospheric basal temperature, κ is the thermal diffusivity, and d_0 is the depth for adiabatic heating. Considering that the youngest seafloor age of the trench is at least 30 Ma, the subduction duration is formulated to be at least $\geq$ 20 Myr to ensure a steady thermal state with a temperature variation $<$10 °C over time.

The dominant rock type in the mantle wedges and the uppermost oceanic mantle consists of ultramafic mantle rocks as harzburgite (olivine + orthopyroxene) represents, and depleted lherzolite (olivine + orthopyroxene + clinopyroxene) is considered subordinate [8]. Seismological studies support the hypothesis that harzburgite represents the principal rock type in the upper mantle. The observed P wave speeds from White et al. [18] for oceanic lower crust and mantle compared with P wave speeds for various rocks at 200 MPa [8] indicate that most oceanic uppermost mantle (suboceanic mantle) velocity measurements are best explained in terms of spinel harzburgite mantle composition. For the above reasons, in our petrological modeling approach, harzburgite is assumed to be the dominant ultramafic rock.

The surface heat flow and Curie depth are correlated, following a theoretical thermal conduction relationship:

$$Q_s = K\frac{T_c - T_0}{Z_b - Z_s} + h_r^2 H_0 \frac{e^{\frac{-Z_b}{h_r}} - e^{\frac{-Z_s}{h_r}}}{Z_b - Z_s} + h_r H_0 e^{\frac{-Z_s}{h_r}} \tag{13}$$

where Q_s is the surface heat flow, T_c is the Curie temperature at the Curie depth Z_b, T_0 is the temperature at the surface elevation Z_s, K is the average thermal conductivity of the magnetic layer, H_0 is the heat production rate at the surface, and h_r is the characteristic drop-off of heat production. The equation shows a nonlinear inverse relationship between heat flow and Z_b [17]. High heat flow measurements tend to correlate with small Curie depths, and vice versa. Synthetic modeling suggests that the largest error in estimated Curie depths using the linearized centroid method will not reach 35%, and the uncertainty of the surface heat flow is expected to be $<$ 20 mW/m^2 due to selected fractal exponent and wavenumber bands for linear regressions and observed surface heat flow in plate convergence zones.

The model is constrained by observations of surface heat flow from the global heat flow database [19] and heat flow values from Curie point depth estimates [20]. The resolution was tested and showed that the temperature variance was $<$ 10 °C when the mesh size exceeded 80 $\times$ 80 $\times$ 100. To investigate the robustness of the model, sensitivity tests are performed, and the mantle viscosity varies from 0.9 $\times$ 10^{20} Pa s to 1.1 $\times$ 10^{20} Pa s and mantle density varies from 3250 kg/m^3 to 3350 kg/m^3. Thus, the benchmark model is presented as deviations from the reference models (ΔT and ΔH_2O) at different depth levels within the subducted oceanic plate. The tests show that mantle density variations ($\pm$50 kg/m^3) induce small temperature variations of $<$10 °C at depths. The model settings combine the simulation methods used in circum-Pacific convergence zones, such as the reconstruction of oceanic-continental cold subduction in Japan [1]. Based on thermomechanical models, the three-dimensional hydrothermal data of various subduction zones, including Alaska, can be obtained.

Ethics Statements

The data have no personal information or institutional references that may compromise the privacy of any parties. It is entirely anonymous; therefore, no ethical implications should be declared.

CRediT Author Statement

Yingfeng Ji: Conceptualization, Methodology, Software, Data curation, Validation, Writing – review & editing, Supervision; **Rui Qu:** Writing – original draft, Visualization, Investigation; **Weiling Zhu:** Validation, Writing – review & editing.

Declaration of Competing Interest

The authors declare that they have no known competing financial interests or personal relationships that could have appeared to influence the work reported in this paper.

Acknowledgments

We are grateful to P. Tackley for sharing the Stag3d code developed in this study. We appreciate the earthquake catalog from IRIS [3]. Figures were created by Paraview software developed by Kitware Inc. This study benefited from financial support from the Second Tibetan Plateau Scientific Expedition and Research Program (2019QZKK0708) and the CAS Pioneer Hundred Talents Program.

References

[1] Y. Ji, S. Yoshioka, T. Matsumoto, Three-dimensional numerical modeling of temperature and mantle flow fields associated with subduction of the Philippine Sea plate, southwest Japan, Journal of Geophysical Research: Solid Earth 121 (2016) 4458–4482.
[2] Y. Ji, S. Yoshioka, V.C. Manea, M. Manea, T. Matsumoto, Three-dimensional numerical modeling of thermal regime and slab dehydration beneath Kanto and Tohoku, Japan, J. Geophys. Res. solid earth 122 (2017) 332–353, doi:10.1002/2016JB013230.
[3] C. Trabant, A.R. Hutko, M. Bahavar, R. Karstens, T. Ahern, R. Aster, Data products at the IRIS DMC: Stepping stones for research and other applications, Seismol. Res. Lett. 83 (2012) 846–854.
[4] G.P. Hayes, G.L. Moore, D.E. Portner, M. Hearne, H. Flamme, M. Furtney, G.M. Smoczyk, Slab2, a comprehensive subduction zone geometry model, Science 362 (2018) 58–61.
[5] C. DeMets, R.G. Gordon, D.F. Argus, Geologically current plate motions, Geophys. J. Int. 181 (2010) 1–80.
[6] D.F. Argus, R.G. Gordon, C. DeMets, Geologically current motion of 56 plates relative to the no-net-rotation reference frame, Geochem. Geophys. Geosyst. 12 (2011).
[7] R.D. Müller, M. Sdrolias, C. Gaina, W.R. Roest, Age, spreading rates, and spreading asymmetry of the world's ocean crust, Geochem. Geophys. Geosyst. 9 (2008).
[8] B.R. Hacker, G.A. Abers, S.M. Peacock, Subduction factory 1. Theoretical mineralogy, densities, seismic wave speeds, and H2O contents, Journal of Geophysical Research: Solid Earth 108 (2003).
[9] T. Yoshii, Regionality of group velocities of Rayleigh waves in the Pacific and thickening of the plate, Earth Planet. Sci. Lett. 25 (1975) 305–312.
[10] C.J. Grose, J.C. Afonso, Comprehensive plate models for the thermal evolution of oceanic lithosphere, Geochem. Geophys. Geosyst. 14 (2013) 3751–3778.
[11] L. Siebert, T. Simkin, P. Kimberly, Volcanoes of the World, Univ of California Press, 2011.
[12] T. Omori, K. Watanabe, R. Umetsu, R. Kainuma, K. Ishida, Martensitic transformation and magnetic field-induced strain in Fe–Mn–Ga shape memory alloy, Appl. Phys. Lett. 95 (2009) 082508.
[13] P. Tackley, S. Xie, STAG3D: A code for modeling thermochemical multiphase convection in Earth's mantle, in: K.J. Bathe (Ed.), Computational fluid and solid mechanics, Elsevier B.V, Amsterdam, 2003, pp. 1524–1527.
[14] E.R. Burkett, M.I. Billen, Three-dimensionality of slab detachment due to ridge-trench collision: Laterally simultaneous boudinage versus tear propagation, Geochem. Geophys. Geosyst. 11 (2010).
[15] G. Hirth, D. Kohlstedf, Rheology of the upper mantle and the mantle wedge: A view from the experimentalists, Geophysical monograph-american geophysical union 138 (2003) 83–106.
[16] G. Ranalli, Rheology of the Earth, Springer Science & Business Media, 1995.
[17] D.L. Turcotte, G. Schubert, Geodynamics, Cambridge university press, 2002.
[18] R.S. White, D. McKenzie, R.K. O'Nions, Oceanic crustal thickness from seismic measurements and rare earth element inversions, Journal of Geophysical Research: Solid Earth 97 (1992) 19683–19715.
[19] H.N. Pollack, S.J. Hurter, J.R. Johnson, Heat flow from the Earth's interior: analysis of the global data set, Rev. Geophys. 31 (1993) 267–280.
[20] C.F. Li, Y. Lu, J. Wang, A global reference model of Curie-point depths based on EMAG2, Sci. Rep. 7 (2017) 1–9.